Optimization of a Dual-Band, Printed Octafilar Antenna

Joseph D. Majkowski

L3Harris Communication Systems
Rochester NY, 14610, United States
Joe.Majkowski@L3Harris.com

Abstract ─ This paper presents several innovative techniques for the design and optimization of a dual band, octafilar helix antenna. The technical challenge of this design is how close the two bands of operation are, as well as the requirement to fit inside a radome with .07λ diameter and .33λ length. This was achieved through a novel technique of applying differing pitches and terminations to the upper and lower frequency antenna filars and then feeding them from a similar location at the base. This allowed for optimal current distribution on each of the two antenna filars. The final design produced gain greater than 0dBic at zenith across both bands of operation. The techniques discussed in this paper were seen to grow low frequency performance by as much as 2.5dBic over a typical octafilar design of the same size.

Index Terms ─ Dualband, octafilar, QHA.

I. INTRODUCTION

Satellite communications have seen continuous growth in the past few decades as we continue to develop and place new constellations in space. These constellations can vary in operational frequencies, type of orbit, and years of service. As the frequency spectrum becomes ever more crowded, the need for close frequency, dual banded structures continue to rise. These antennas must meet strict performance standards to close communication links with geostationary earth orbit or geosynchronous equatorial orbit (GEO) satellite constellations. These constellations are located at altitudes of approximately 35786 kilometers, (22236 miles), above mean sea level. Given the large propagation distance, path loss is very high, which gives rise to the need for high-performance antennas to close the links.

The quadrafilar helix antenna, (QHA), is a prime candidate for utilization in such communication links. The advantages of these antennas lie in their cardioid shaped pattern, low axial ratio, and high right-hand circular polarization (RHCP) gain [1]. Another main advantage of QHA antennas is ability to produce a forward firing antenna which is independent of the ground plane presented. This gives the antenna significantly better performance over circularly polarized microstrip patch antennas which quickly lose desired performance without an electrically large ground plane [2] The QHA also exhibits an advantage in terms of low angle elevation performance. Typically, the wrapping of the elements can be reduced to increase low angle elevation performance at the cost of gain at zenith.

As satellite communications grew so too did the need for wide bandwidth, increased performance, multiple bands of operation and small form factor antennas. This led to the evolution of antennas such as the QHA by adding multiple filars [3,4]. This configuration can extend or add bandwidth and even enhance performance but does little to affect size.

Multiple techniques were explored to help decrease the size of these antennas. These techniques were the DMFA (Dielectric Multi-filar helical antenna) and the PMFA (Printed Mult-filar helical antenna). The DMFA utilizes high ε_R to shrink the overall package size [3,4]. While effective, this typically will result in a decrease in bandwidth as well as decreased efficiency. The PMFA allows for a broad scope of artwork to be employed for the filars. This has led to utilization of differing meandering techniques such as fractals and folded arms [5,6]. Printing has also allowed for the use of rigid boards to make shapes outside of a cylinder, such as the square shaped QHA [7].

The more traditional wire-based elements explore other techniques to improve performance. Such techniques include small matching networks both at the element feeds and at the top of the elements [8,9]. These methods help to add more bandwidth to the antenna, but are limited due to the poor radiation resistance of the structure. To achieve a second band of operation two separate quadrifilars, with differing lengths and circumferences, were nested inside one another to reduce size [10]. Another design provided a switching diode to change electrical length of the element and switch between two modes of operation [11].

In this paper, a novel, dual quadrifilar or octafilar is designed, fabricated and measured. The two filar structures, which occupy the same circumference, have separate termination points which allows for proper

Submitted On: May 28, 2019
Accepted On: October 28, 2019

resonant length to be set individually for each loop. The high frequency and low frequency filar structures are also set at differing pitch angles to maximize isolation of the two nested QHA while maintaining a low frequency coupling factor to improve low frequency impedance. The high frequency band structure's orthogonal elements also needed to be electrically isolated from one another to prevent improper current distribution from occurring. The antenna structure itself was fed with a 90-degree hybrid and two phase matched baluns. Finally, a fiberglass radome was custom designed and utilized to house the final antenna. Details of the final antenna are shown and described along with both experimental and numerical results.

II. QHA ANTENNA BACKGROUND

The QHA, in one form or another, has been around for decades in the satellite communication world. It is utilized primarily for its ease of implementation, high gain, and ability to customize both pattern width and polarization.

The QHA can be approximated as two orthogonal loops. Like a loop, these structures have low radiation resistance which makes them very hard to match and thus even more challenging to achieve wide bandwidths. The overall antenna efficiency and radiation performance is closely tied to overall antenna size characteristics. The general trend is the wider the diameter of the QHA, the wider the bandwidth, the higher the radiation resistance, and ultimately the more efficient the antenna is. This will be the trend until the diameter QHA approaches λ/4 of the intended frequency. These trends are explained graphically for helical antennas in Fig. 1 as well as empirically through equations (1-3). Equations (1-3) show that the circumference of helical antennas is the largest contributing factor to antenna performance. The Red dot on Fig. 1 shows where the antenna in this paper lies upon the chart. From Fig. 1 it is seen that the designed antenna is roughly one-third the size of a typically designed octafilar antenna:

$$Z_{in} \approx 140 * \frac{C}{\lambda}, \tag{1}$$

$$G \approx \frac{6.2*C^2*N*S*f^3}{c^3} - (-10 * \log(1-\Gamma^2)), \tag{2}$$

$$HPBW \approx \frac{65\lambda}{C\sqrt{\frac{NS}{\lambda}}}. \tag{3}$$

Upon further inspection of Fig. 1, the ideal circumference for QHA and octafilar designs is seen to be between .8λ and 1.2λ with a spacing of 1λ – 1.6λ and a pitch angle between 45 and 60 degrees. The optimal width/length design for helical antennas sits around 1/2. These parameters allow for excellent input impedance, gain, and HPBW. However, once the size of the antenna starts to shrink, especially the circumference, the input impedance will drop significantly. This can be seen in Fig. 2 with the red dot marking the size of the antenna in this paper. The input impedance of the lower frequency loop is seen to be very low, sitting at about 6 ohms.

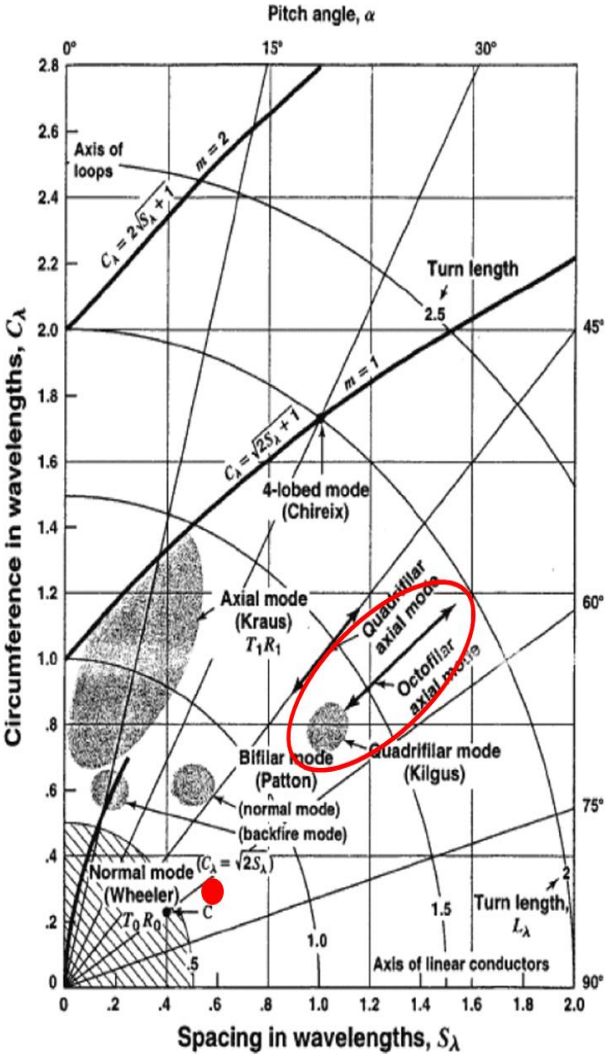

Fig. 1. Helical Mode Chart (reproduced from [12]).

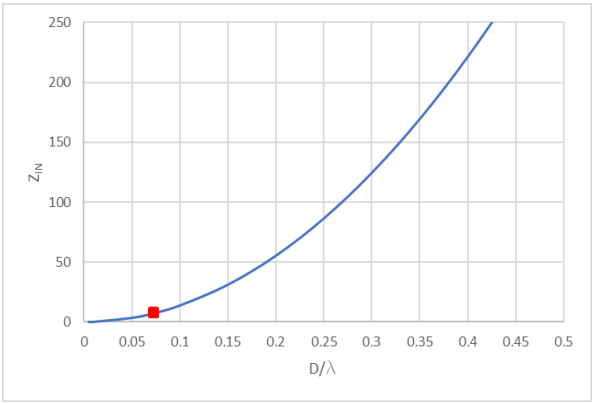

Fig. 2. Input impedance as a function of helix diameter.

To achieve maximum radiation with a QHA structure the elements need to be balanced and fed 90 degrees out of phase. The elements are designed such that RF current peaks occur at the far ends of the cylindrical structure. Following this the voltage should be inversed of the current and produce a peak halfway along the structure. This distribution allows for the cardioid shape pattern and high peak gain values. An HFSS simulation was performed on an ideal QHA to demonstrate the current and voltage distribution [13]. The results can be seen in Fig. 3.

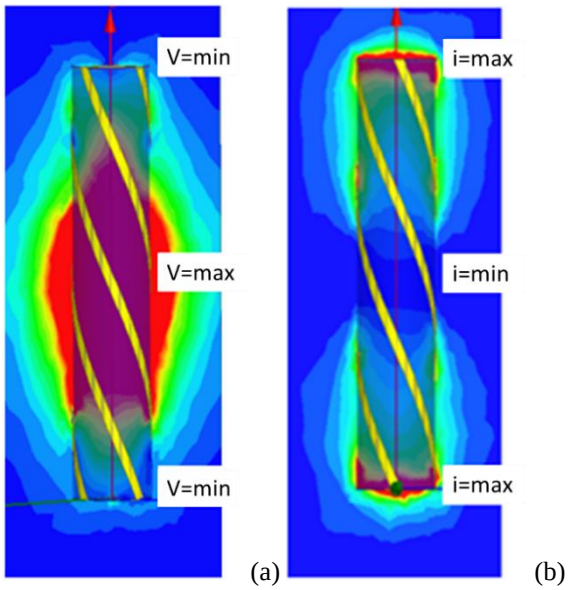

Fig. 3. Colored contour plots showing proper radiation for a QHA at resonance for: (a) voltage (V/m) and (b) current (A/m).

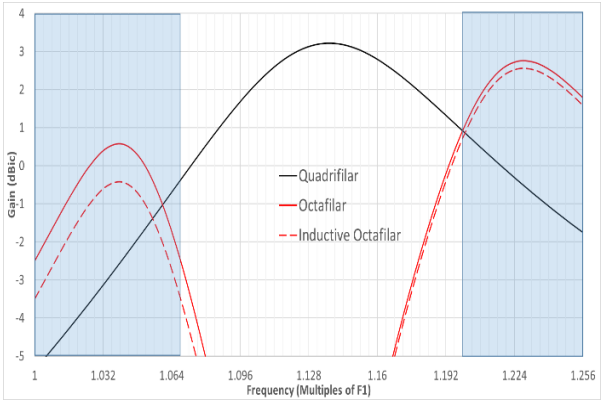

Fig. 4. Simulation results comparing standard quadrifilar, octafilar, and inductively loaded octafilar design gains with a .07λ diameter.

Due to the size restriction of the proposed antenna, an HFSS simulation was performed on an ideal QHA, octafilar, and inductively loaded octafilar design in HFSS at the necessary .07λ diameter. The peak gain results at zenith of these three simulations are compared in Fig. 4. The graph expresses the frequency in terms of multiples of the lowest operating frequency, F1.

The octafilars were simulated with an ideal 45 degree spacing between all elements. The octafilar had a separation in heights of the high and low frequency elements whereas the loaded octafilar had the same termination point for the low and high frequency elements. The quadrifilar is seen to have a narrow bandwidth and fall well below the necessary 0dBic gain performance. In fact, the QHA is seen to only rise above the 0 dBic threshold in the area of band separation. Thus, the QHA would be a poor choice for this application due to its bandwidth limitation.

The octafilar produces better performance in the two separated bands of operation but will need modifications in order to improve performance above the necessary 0dBic threshold. The inductively loaded octafilar is slightly shorter and is forced to go resonant at the high frequencies via inductive loading. This causes even more degradation in the low frequency band of operation due to the smaller overall size of the antenna. Thus the inductively loaded octafilar is a poor choice for this application as it only reduces the height of the antenna and produces even lower efficiency in the low frequency band.

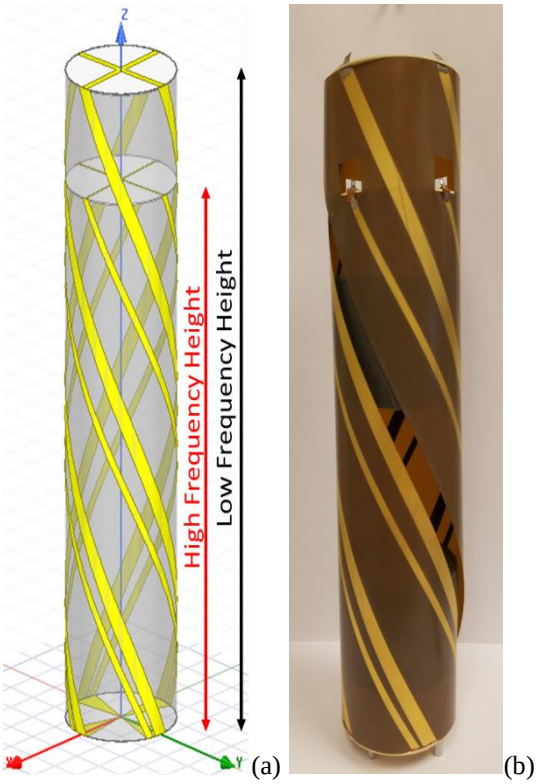

Fig. 5. Image of antenna for: (a) HFSS model and (b) as built.

The designed octafilar can be seen in Fig. 5 and Fig. 6 with dimensions. The antenna has two differing lengths of filars, each fed from a singular point at the base. The low frequency total height is .33λ while the high frequency height is .275λ. The low and high frequency elements each have their own pitch angle set at 63° and 60° respectively which causes them to complete roughly .75 of a complete revolution. Finally, the higher frequency structure has the perpendicular arms DC isolated from each other with a small via connected trace to the back of the rigid PWB.

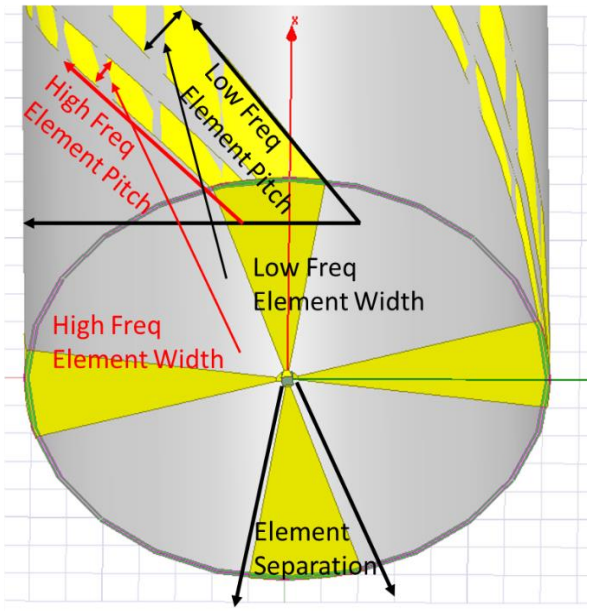

Fig. 6. HFSS image of feed of antenna with dimensions.

III. SEPERATED LOOP HEIGHTS

An HFSS simulation was performed comparing the relative gain performance of a quadrifilar, an octafilar, and an inductively loaded octafilar. This comparison is seen in the plot in Fig. 4. By forcing the antenna to become resonant with methods such as inductors or meandering, the overall performance of the low frequency element is degraded.

To setup proper voltage and current distribution, the high and low frequency elements were each set to differing heights. This height difference allowed for each element to naturally reach its proper electrical length. Naturally reaching proper electrical length enables the structure to radiate properly in each band, producing the cardioid shaped pattern. Completing the loops at differing heights also allowed for each element thickness, height, and crossing structure to be fine-tuned which allow for the performance of each structure to be finely controlled.

As seen in Fig. 5 the structure was constructed utilizing rigid PWBs (Printed Wiring Board) that soldered directly onto the FWB (Flexible Wiring Board) on which the main filars were printed. The PWB/FWB method allows for the dimensions of each structure to be finely controlled while maintaining a quick, easy, and controllable production method.

During the design process it was discovered that the high and low frequency termination points have a coupling correlation. It was found through parametric study that the optimum delta between the completion of the loops was set at a .05λ spacing. As the spacing began to grow or shrink outside of that distance the gain of the structure was adversely affected.

IV. DIFFERING PITCHED ELEMENTS

Upon inspection of the numerical results it is found that an octafilar with a small diameter still has ideal gain. However, the end performance lacks due to the mismatch loss that is presented by the low impedance structure of the antenna. The initial untuned antenna was seen to have low frequency impedance of 6 ohms.

The model was constructed in HFSS utilizing perfect E sheets wrapped around a cylinder. Modeling the structure in this method helped to speed up computational time as well as prevent non-manifold edges from occurring in the model. The model was found to be very close to a thickened sheet version of the model.

Parametric sweeps were run with this model to look at the impedance of the structure as the angle of separation between the high and low frequency structure was varied. This was further elaborated by also varying the angle at which the low frequency element was wrapped. This was characterized in Fig. 7 as ext pitch to signify that the low frequency element pitch is X degrees more than the high frequency element pitch. Changing the pitch of the low frequency element with respect to the high frequency element allows for the separation between the two elements to grow as the antenna element length is traversed. This will present more coupling toward the feed of the antenna while reducing coupling further away from the feed of the elements.

Figure 7 (a) shows that the closer the elements become, or the lower their separation, the higher the impedance gets for the low frequency structure. The low frequency structure gets to 22 ohms with a separation of 25 degrees. This phenomenon is also followed by an inductive detuning that causes the structure to resonate a little lower in frequency. Figure 7 (b) shows a slightly less dramatic but opposite effect in impedance, dropping down from 13 ohms to 11 ohms at 25 degrees of separation. This is also accompanied by an inductive detuning of the antenna.

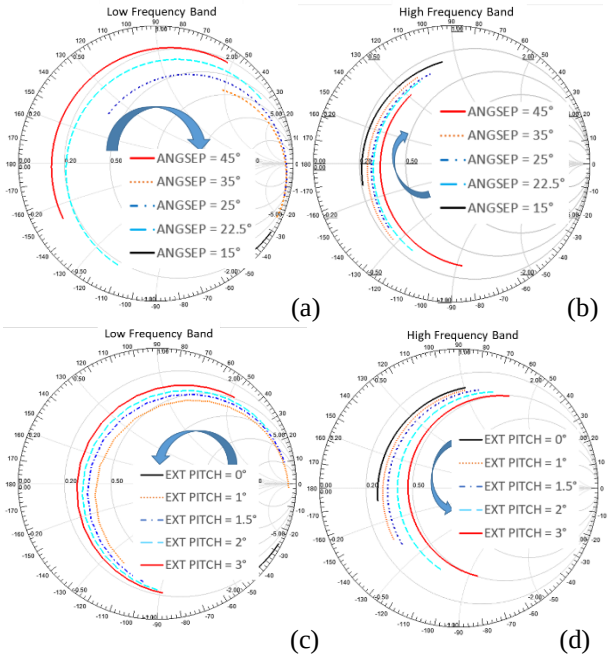

Fig. 7. Impedance charts for varying: (a) angle of seperation at base of element in low frequency band, (b) angle of seperation at base of element in high frequency band, (c) extra pitch angle applied to high frequency element in low frequency band, and (d) extra pitch angle applied to high frequency element in high frequency band.

The low frequency structure pitch angle was then varied while keeping the high frequency structure pitch angle constant. Figure 7 (c) shows the impedance of the low frequency structure decreasing from 22 ohms to 17 ohms while losing a large amount of the inductance introduced by decreasing the element separation. Figure 7 (d) shows the high frequency structure impedance doing the opposite and increasing in resistance by about 10 ohms while also losing the inductive loading introduced by bringing the elements closer together.

Thus, a balance of the two techniques allows for an increase in Low band impedance by about 15 ohms while only negatively affecting the high frequency band by 2 ohms. This translates to about a 2.5dB improvement in low frequency band performance while only adversely affecting the high frequency band by about .5dB.

V. UNEVEN CURRENT DISTRIBUTIONS

Due to the proximity of both the high frequency and low frequency crossing points a coupling issue is introduced onto the high frequency structure. This coupling causes a current imbalance to occur, forcing most of the current at high frequency onto a single filar. This uneven current distribution phenomenon can be seen in Fig. 8. Current from 3 of the copper traces all combine to go down the farthest right copper trace. The distribution causes a 1-2 dB drop in performance to occur over 30% of the high frequency band as seen in Fig. 9.

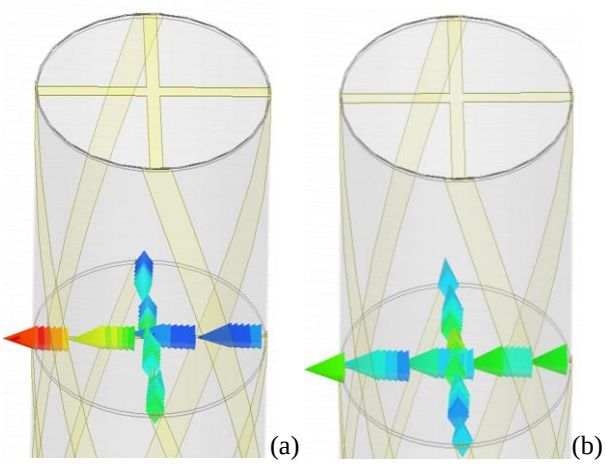

Fig. 8. Image of current distribution on high frequency element termination: (a) DC connected and (b) DC isolated.

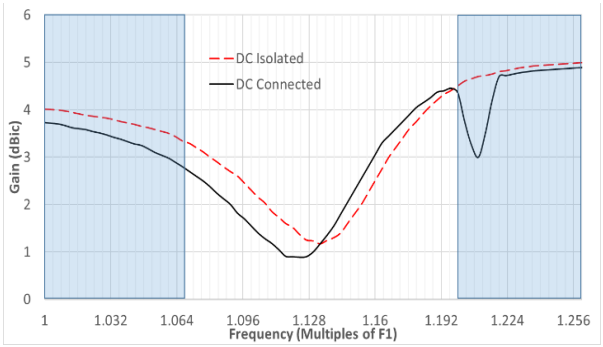

Fig. 9. Simulation of gain at zenith of antenna with high frequency 0° and 90° elements DC connected and DC isolated.

To prevent the unwanted combination of currents on the traces, the crossing point of the high frequency structure was DC isolated from one another as seen in Fig. 10. This was realized by taking the horizontal trace and creating two via points to bring the trace to the back of the rigid PWB and run underneath the vertical element.

DC isolation is a bit counterintuitive to solve the problem. Typically, the traces are combined to force equal current distributions to occur on the filars. However, in this configuration this special technique is necessary to reduce the coupling between high and low frequency elements and thus retain performance.

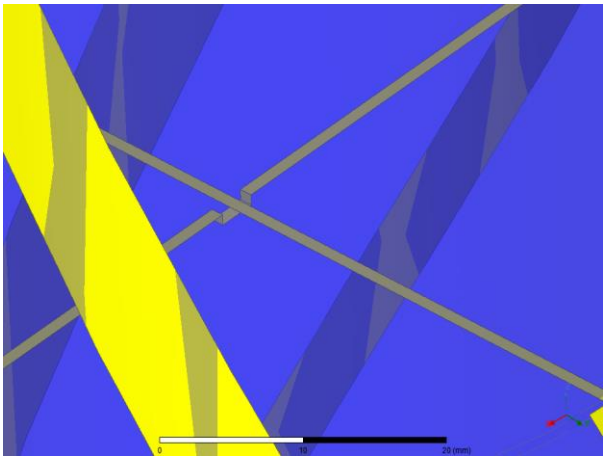

Fig. 10. Close up HFSS image of high frequency crossover point with DC Isolation.

VI. FEEDING STRUCTURE AND RADOME

The antenna structure was fabricated on a 4-mil thick piece of Dupont® Pyralux AP 9141R with a dielectric constant of 3.3. Tabs were created to be able to insert directly into the rigid PWBs that controlled the crossing points of the loops. The boards were then simply soldered into place with the excess tab being clipped off. The FWB not only allowed for ease of manufacturing but also allowed for accurate dimensions to be rendered on the final antenna. This whole assembly was then inserted into a radome which could withstand the rigors of MIL STD 810-G testing.

A 1/32" wall thickness cylinder of fiberglass was chosen as a radome due to its structural integrity, good electrical properties and customizable size. However, once the radome was affixed to the antenna structure, significant dielectric loading was seen. This loading also seemed to vary proto-type to proto-type and test to test. The main source of variance was due to irregularities in how the antenna cylinder was formed, thus leading to varying dielectric loading unit to unit. To get maximum consistency, as well as mechanical integrity, an oversized section of polyurethane foam was inserted as the core of the antenna element. The dielectric associated with such a material is typically around 1.02-1.05 depending upon material density and manufacturing techniques of the foam. Thus, it had minimal effects upon the overall antenna performance but helped to increase maximum contact to the radome structure creating a consistent dielectric loading unit to unit. The shift in frequency due to dielectric loading of the fiberglass was .05λ. A small portion of this radome can be seen in Fig. 11.

The antenna was fed with an Anaren® Xinger 90-degree hybrid coupler. The hybrid was outfitted with a 20-watt resistor to handle maximum transmitter power. This hybrid not only feeds the two antenna elements 90 degrees out of phase but also will provide a VSWR of under 1.5:1 across the band. The hybrid and 50-ohm load were mounted to a PCB as seen in right side of Fig. 10. The PCB was then attached to a large aluminum radome adaptor that also acts as a heat sink for any heat generated in the 50-ohm load.

A pair of phase matched Baluns are then utilized to feed the antenna to the 90 degree hybrid. This will serve the purpose of helping to isolate the antenna while also maintaining the necessary phase offset when feeding.

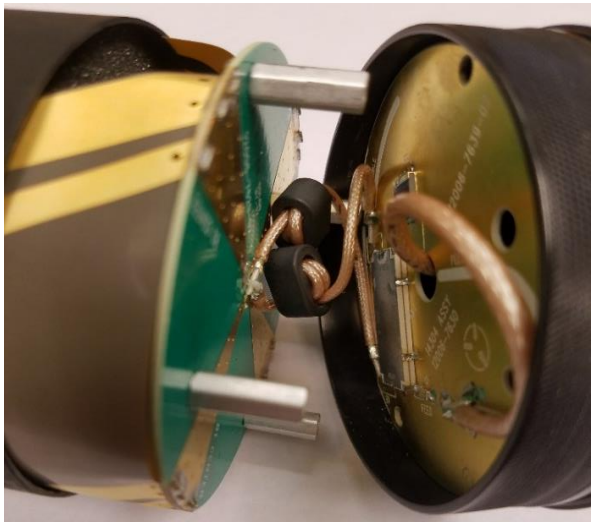

Fig. 11. Image of the feed structure and radome of proto-type antenna.

VII. RESULTS

The antennas were measured in a 5-meter by 3-meter anechoic chamber. All measurements were taken utilizing an Agilent E5017B network analyzer. The turntable utilize for patterns is an ETS Lindgren 2188, 1.2-meter diameter turntable with ETS 2090 controller. Finally, all gain measurements were taken utilizing the 3-antenna technique with antennas from the A.H. Systems AK-4G calibrated antenna kit and TDS-535-2 calibrated dipole kit.

The smith chart can be seen in Fig. 12. The return loss can be seen in Fig. 13. Overall the performance of the antenna matches shape closely with simulation but has a higher resistance. This discrepancy can be accounted for by the addition of the baluns for measurement as well as the losses associated with the radome. The contact with the radome is nonideal and creates small air gaps that do not exist in the model. The model was also constructed using Perfect E sheets, to speed up the simulation, which do not properly reflect the losses associated with copper on an FWB. However, the simulation and measurement both agree that the antenna is resonant slightly above and below the center frequency of the lower and upper frequency bands respectively. This is necessary to achieve peak gain at

the center of each frequency band.

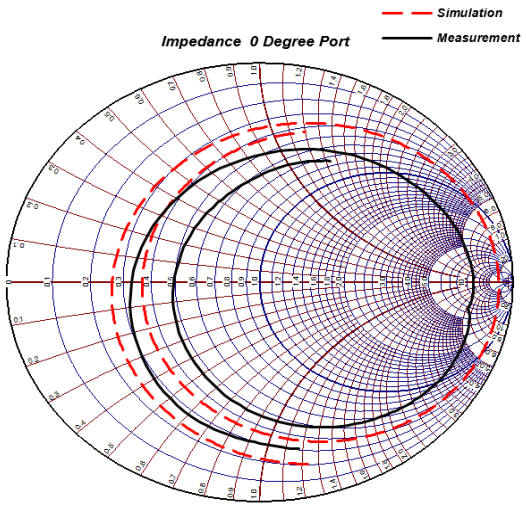

Fig. 12. Smith chart of 0 degree port of antenna elements.

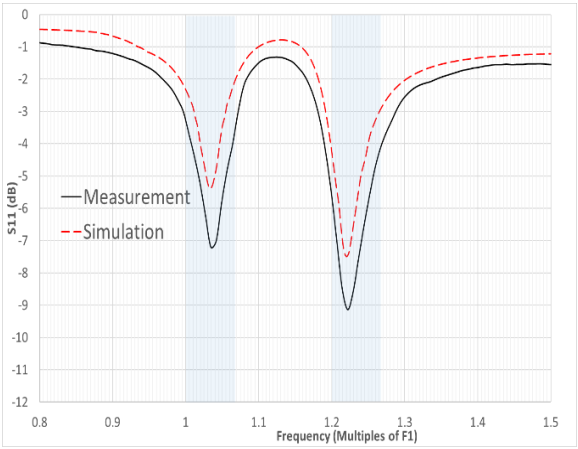

Fig. 13. Return loss of 0 degree port of antenna elements.

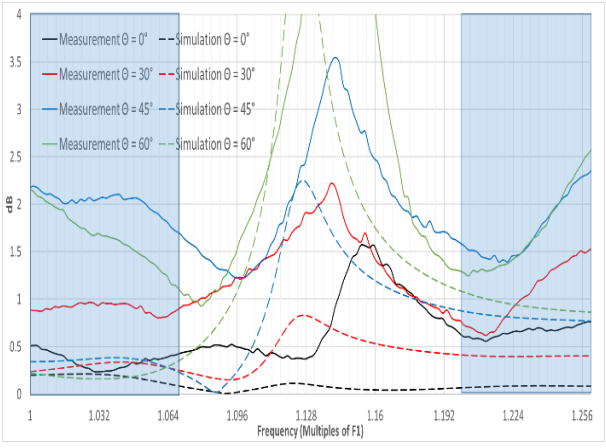

Fig. 14. Axial ratio of antenna at varying elevation angles.

The axial ratio of the antenna at varying elevation angles can be seen in Fig. 14. Both the model and the simulation show acceptable axial ratio at low elevation angles in the bands of operation. However, the measurement shows a steeper increase in axial ratio as elevation angle decreases than that of the model. This difference in measurement result can be attributed to the imperfect construction of the antenna verses a perfectly constructed and balanced numerical model. The 90-degree hybrid utilized for measurements verses the ideal phase shifter utilized in the model will also cause shifts in the axial ratio. These differences will be most prominent at the antenna and device band edges where phase imblance is typically at the highest acceptable level for the device. This is especially true at the highest frequency where phase inblance will of course be the highest.

Gain patterns at the middle of each band of the antenna can be seen in Fig. 15 and Fig. 16 with a comparison of peak gains seen in Table 1. Simulation and measurement are very comparable across both bands of operation. The peak delta is about 1 dB and can be accounted for by the addition of the real world hybrid in the antenna to achieve circular polrization as well as the outside elements such as the baluns, heatsink, and gooseneck.

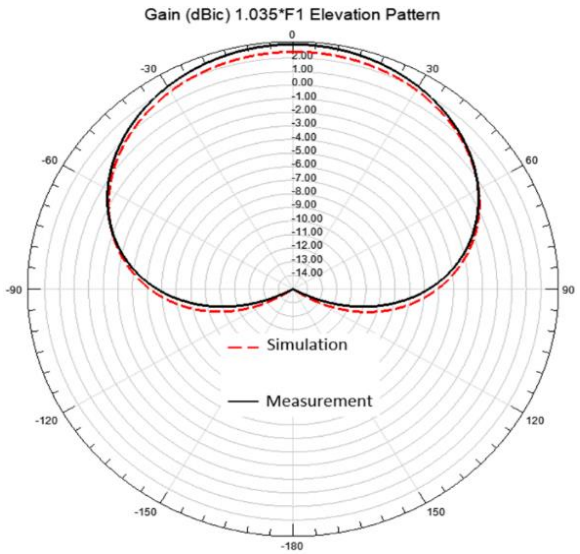

Fig. 15. Radation patten comparison of low frequency band for 1.035*F1.

The maximum gain of the antenna is perfectly centered at Zenith and realizes the goal of greater than 0 dBic across the lower frequency band, peaking out at 3dBic. The same can be said of the upper frequency band where the goal of greater than 2dBic is met across the upper frequency band with a peak of 3.5dBic.

The patterns are incredibly wide and exhibit a

excellent HPBW of ±60˚ off of zenith. This good low elevation angle gain is beneficial to forming terrestrial links. Overall the patterns agree numerical to measurement very well across both bands of operation from both a shape, gain and HPBW perspective. It is seen in Table 1 that the majority of the the optimized octafilar benefit occurs at the low frequency band where impedance was optimized. This translated to at least a 2.5 dBic improvement over the other techniques.

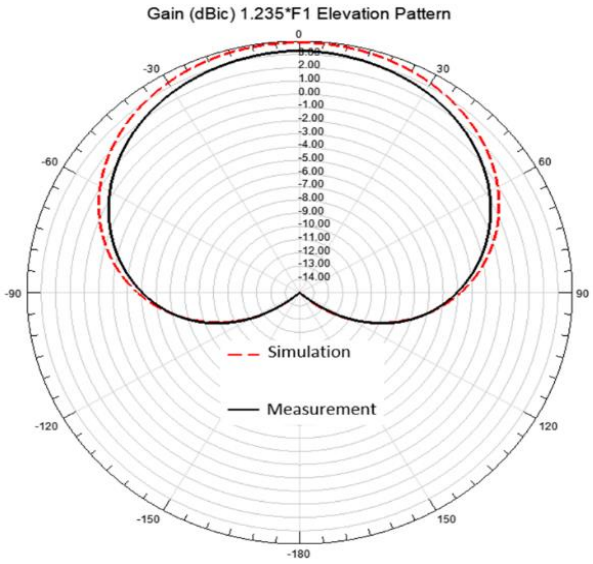

Fig. 16. Radation patten comparison of high frequency band for 1.235*F1.

Table 1: Comparison of peak gain at zenith of various QHA designs

Frequency (λ) / Gain(dBic)	1	1.035	1.07	1.2	1.235	1.27
Quadrifilar (Numerical)	-5.37	-2.73	-0.48	0.91	-0.76	-2.18
Octafilar (Numerical)	-2.503	0.45	-2.22	0.94	2.71	1.17
Inductive Octafilar (Numerical)	-3.5	-0.55	-3.22	0.74	2.51	0.97
Optimized Octafilar (Numerical)	-0.05	2.45	0.65	2.31	3.89	2.51
Optimized Octafilar (Measurement)	0.34	3	0.22	2.07	3.27	2.49

VIII. CONCLUSION

A small diameter, light weight, dual-band octafilar antenna was designed and fabricated for operation over two .07λ bands of operation. The two sets of filars ended up with differing heights of termination to allow for optimal current distributions and peak gain. The two sets of filars also had differing pitches and separation which allowed for improved performance in the low frequency band with minimal degredation on the performance of the high frequency band. The High frequency 0° and 90° crossing point needed to be DC isolated from one another to prevent improper current distribution and hence a decrease in performance.

These novel techniques allowed for equal wraps around the circumference of the tube which created equal shaped cardioid patterns with good low elevation performance. The end antenna was then fed with a 90-degree hybrid and isolated from the mounting structure with phase matched baluns. The resulting antenna was able to provide the necessary high performance in a significantly smaller and lighter weight package size which was acceptable to the end user.

ACKNOWLEDGEMENTS

The author would like to acknowledge Malcolm Packer of L3Harris Communication Systems of Rochester, NY for his help in editing this paper and his constant guidance and support.

REFERENCES

[1] C. A. Balanis, *Antenna Theory*. 3rd Ed., New York: Wiley, pp. 549-600, 2005.

[2] N. M. Tuan, K. Byoungchul, C. Hosung, and P. Ikmo, "Effects of ground plane size on a square microstrip patch antenna designed on a low-permittivity substrate with an air gap," *Antenna Technology (iWAT) 2010 International Workshop on*, pp. 1-4, 2010.

[3] O. P. Leisten, J. C. Vardaxoglou, P. McEvoy, R. Seager, and A. Wingfield, "Miniature dielectrically-loaded quadrifilar antenna for global positioning system (GPS)," Electronics Letters, vol. 37, pp. 1321-1322, 2001.

[4] S. Liu and Q.-X. Chi, "A novel dielectrically-loaded antenna for tri-band GPS applications," *38th European Microwave Conference*, 2008.

[5] A. Takacs, H. Aubert, D. Belot, and H. Diez, "Miniaturization of compact quadrifilar helix antennas for telemetry, tracking and command applications," *Progress In Electromagnetics Research C*, vol. 60, pp. 125-136, 2015.

[6] A. Petros and S. Licul, "Folded quadrifilar helix antenna," in *IEEE Antennas and Propagation Symposium*, v. 4, pp. 569-572, 2001.

[7] W. I. Son, H. Tae, and J. Yu, "Compact square quadrifilar helix antenna for SDARS application in portable terminals," *Electronics Letters*, vol. 47, no. 4, pp. 232-233, 2011.

[8] M. Hosseini, M. Hakkak, and P. Rezaei, "Design of a dual-band quadrifilar helix antenna", *IEEE Antennas Wireless. Propagation. Lett.*, vol. 4, pp.

39-42, 2005.
[9] D. Lamensdorf and M. A. Smolinski, "Dual band quadrifilar helix antenna," *Proc. IEEE Int. Symp. Antennas and Propagation*, vol. 3, pp. 488-491, 2002.
[10] J. Lowdell, G. Cox, M. Notter, and K. Keen, "Dual band quadrifilar helix antennas for UHF/VHF band operation," presented at the *ICAP*, Exeter, 2003.
[11] A. Sainati, A. Robert, J. J. Groppelli, R. C. Olesen, and A. J. Stanland, "A band-switched resonant quadrifilar helix," *IEEE Trans. Antennas Propag*., vol. AP-30, no. 5, pp. 1010-1013, Sep. 1982.
[12] J. D. Kraus, *Antennas*. McGraw-Hill, 1988.
[13] Ansoft High Frequency Structure Simulator (HFSS), ver. 17, Ansoft Corporation, Pittsburgh, PA, 2017.

Joseph Daniel Majkowski received his B.S. and M.S. degrees in Electrical Engineering from the Rochester Institute of Technology in 2012.

He joined Harris Communications in 2012 where he began as a System Engineer. In 2013 he changed roles within the company to an Electromagnetic Engineer position. He has since won corporate wide technological innovation awards in 2017 and 2018 for his work in matching circuits and antenna design. This work has led to four patent filings to date. He was also the chair of the IEEE Rochester section MTT17/AP03 society in 2018.